J. Am. Soc. Mass Spectrom. (2018) 29:1892–1900
DOI: 10.1007/s13361-018-1985-z

RESEARCH ARTICLE

Carbon Nanoparticles and Graphene Nanosheets as MALDI Matrices in Glycomics: a New Approach to Improve Glycan Profiling in Biological Samples

Alireza Banazadeh, Wenjing Peng, Lucas Veillon, Yehia Mechref

Department of Chemistry and Biochemistry, Texas Tech University, Lubbock, TX 79409-1061, USA

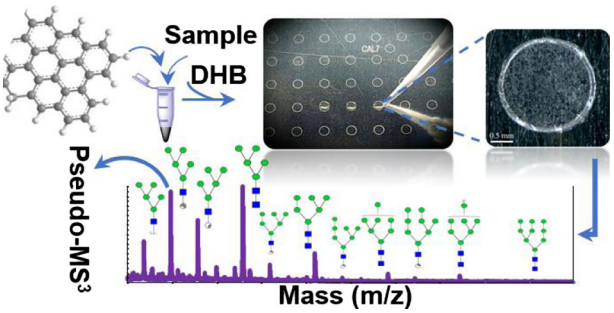

Abstract. Glycomics continues to be a highly dynamic and interesting research area due to the need to comprehensively understand the biological attributes of glycosylation in many important biological functions such as the immune response, cell development, cell differentiation/adhesion, and host-pathogen interactions. Although matrix-assisted laser desorption ionization (MALDI) mass spectrometry (MS) has proven to be suitable for glycomic profiling studies, there is a need for improved sensitivity in the detection of native glycans, which ionize inefficiently. In this study, we investigated the efficiencies of graphene nanosheets (GNs) and carbon nanoparticles (CNPs) as MALDI matrices and co-matrices in glycan profiling. Our results indicated an enhancement of signal intensity by several orders of magnitude upon using GNs and CNPs in MALDI analysis of N-glycans derived from a variety of biological samples. Interestingly, increasing the amounts of CNPs and GNs improved not only the signal intensities but also prompted in-source decay (ISD) fragmentations, which produced extensive glycosidic and cross-ring cleavages. Our results indicated that the extent of ISD fragmentation could be modulated by CNP and GN concentrations, to obtain MS^2 and pseudo-MS^3 spectra. The results for glycan profiling in high salt solutions confirmed high salt-tolerance capacities for both CNPs and GNs. Finally, the results showed that by using CNPs and GNs as co-matrices, DHB crystal formation was more homogeneous which improved shot-to-shot reproducibility and sensitivity.

Keywords: Nanoparticles, Graphene, MALDI-MS, Glycans

Received: 9 March 2018/Revised: 28 April 2018/Accepted: 28 April 2018/Published Online: 18 June 2018

Introduction

Glycosylation is one of the most essential post-translational modifications of proteins, which plays a major role in many biological functions, including protein folding, cell division, tumor immunology, and signal transduction. Changes in glycosylation have also been associated with a wide range of human diseases, and the monitoring of such changes can be effectively employed for disease diagnosis and prognosis [1–6]. Therefore, structural identification of glycans, including glycosidic and cross-ring characterization, at high sensitivity is essential for the understanding of their interactions within biological specimens, and also for the evaluation of the therapeutic efficacy of disease treatments.

Among the different analytical methods that have been reported for glycan analysis, MS techniques coupled with a variety of dissociation techniques, including high- or low-energy collision-induced fragmentation (CID), post-source decay (PSD), infrared multiphoton dissociation (IRMPD), electron excitation dissociation (EED), electron capture dissociation (ECD), electron transfer dissociation (ETD), and electron detachment dissociation (EDD), have proven to be a powerful tools for glycan profiling [7–17]. In this regard, MALDI offers several advantages over other ionization techniques, mainly

Electronic supplementary material The online version of this article (https://doi.org/10.1007/s13361-018-1985-z) contains supplementary material, which is available to authorized users.

Correspondence to: Yehia Mechref; *e-mail:* yehia.mechref@ttu.edu

ease of operation, short analysis times, modest sample size requirements, and relative simplicity of spectral interpretation [12, 18, 19]. However, due to the complexity of glycan structures and their low abundance and low ionization efficiency relative to the peptides and proteins, there are still challenges to be addressed in the direct analysis of glycans by MALDI-MS. Therefore, the utilization of novel matrix materials for both the selective enrichment of glycans and the improvement of their ionization efficiencies are necessary to facilitate direct and effective MS measurements of glycans.

Owing to the superior physicochemical characteristics of nanomaterials, their importance has become increasingly evident over the past decade. Among these materials, carbon-based nanomaterials such as graphene nanosheets, carbon nanotubes, and carbon nanodots have attracted the most attention as outstanding MALDI matrices, because of their excellent optical absorption, superior electrical properties, and low background interference [20–28]. Efficient energy absorption and transfer facilitate the desorption process, thus enhancing MS signal intensity compared with traditional organic matrices. The proficiency of these materials can also be enhanced by using binary matrices (e.g., carbon dots/9-aminoacridine and α-cyano-4-hydroxycinnamic ac-id/graphene) which improved detection sensitivity and shot-to-shot reproducibility by producing more homogeneous co-crystallization matrix layers [21, 27]. Carbon nanomaterials have also been demonstrated to be an excellent class of sorbent materials for extraction and enrichment of a variety biological molecules such as amino acids, polyamines, peptides, steroids, DNA, and carbohydrates [22, 25, 28–30].

Even though MALDI is considered a soft ionization process, in-source decay (ISD) still typically occurs in the MALDI source during the ionization process, producing fragment ions that complicate spectra [31]. Although they make interpretation of spectra more complex, they can be helpful in glycan profiling and structural identification. An additional benefit provided by ISD fragmentation is the potential for pseudo-MS^3 experiments. The degree of ISD fragmentation is dependent on matrix materials and laser intensity, and the more control that can be exerted on the process, the more useful it is. Liang et al. studied the effect of iron oxide nanoparticles on the ISD of five model glycans including glucose, sucrose, isomaltotriose, maltoheptaose, and *β*-cyclodextrin [32]. Abundant glycosidic and cross-ring cleavages by ISD were observed, which indicated that the matrix provided strong energy transfer to the sample. However, pseudo-MS^3 analyses and the possibility of controlling the degree of ISD were not investigated. Furthermore, ions representing a loss/gain of 42 Da (CH_2CO) and 60 Da (CH_3COOH) were observed in abundance for both precursor and product-ions, which resulted in more complex MS spectra.

To date, there have been no prior investigations into the potential benefits of utilizing carbon-based nanomaterials as matrices or co-matrices for MALDI-MS analysis of native and permethylated glycans. In this study, we investigated the efficiencies of GNs and CNPs as MALDI matrices and co-matrices for the profiling of glycans from model glycoproteins and human blood serum. Owing to the properties of carbon-based nanoparticles that promote superior absorption of glycans, for purification, and absorption of laser energy, for the transfer of energy to analytes for MALDI-MS analyses, they demonstrate a capacity for multifaceted roles. Further, we are also the first to probe the potential for the use of carbon-based nanoparticles to facilitate pseudo-MS^3 analyses for pure glycan samples.

Experimental Section

Materials

Carbon nanoparticles, graphene nanosheets, ribonuclease B (RNase B), fetuin from bovine serum, human alpha-1 acid glycoprotein (AGP), and human blood serum were purchased from Sigma-Aldrich (St. Louis, MO). Microspin columns were purchased from Harvard Apparatus (Holliston, MA), and PNGase F with 10 × G7 reaction buffer (0.5 M sodium phosphate) was obtained from New England Biolabs (Ipswich, MA). HPLC grade water, ethanol, and acetonitrile (ACN) were used for the preparation of samples.

Sample Preparation Methods

N-Glycans were released from RNase B, fetuin, AGP, and human blood serum according to a previously reported method [16]. Briefly, model glycoproteins or human blood serum were mixed with G7 buffer and denatured in an 80 °C water bath for 30 min. After cooling to room temperature, PNGase F digestion followed in a 37 °C water bath for 18 h. Released N-glycans were purified by precipitation of peptides and proteins by addition of 90% ethanol and incubation at − 20 °C for 30 min. Purified glycans were then reduced and permethylated as described in previous reports [16, 33, 34].

For matrix preparation, CNPs and GNs (2 mg of each) were dispersed in 1 mL of an ethanol/water (1:1, *v*/*v*) solution with sonication for 10 min prior to use. The solutions were then mixed, at concentrations determined to be optimal, with an equal volume of 20 mg mL^{-1} DHB (2,5-dihydroxybenzoic acid) to form binary matrices. A total of 0.5 μL of the resulting suspensions were added to the MALDI plate, followed by the addition of 0.5 μL of the sample solutions. The efficiencies of CNPs, GNs, and DHB as MALDI matrices were also investigated separately by adding 0.5 μl of each matrix solution to the MALDI plate.

Purification of Glycans Using CNPs and GNs

A total of 10 μl of CNP or GN suspensions (0.2 μg $μl^{-1}$ in 10% ACN) was pipetted into a 10-μl aliquot of analyte solutions, which were prepared in 10% aqueous CAN solution. The mixtures were sonicated for 10 min, to facilitate glycan absorption, followed by high-speed centrifugation at 14.8 K rpm for 10 min to collect glycan-loaded CNPs or GNs. The supernatants were removed, and the black aggregates were washed with water and re-suspended in 10 μl of 10% ACN. Finally,

1 μl of the suspensions was mixed with 1 μl of DHB prior to MALDI analysis.

Instrumentation

Transmission electron microscopy (TEM) (Hitachi H-8100) was used to characterize the surface morphology of CNPs and GNs. Raman spectra were measured with a SENTERRA dispersive Raman microscope spectrometer (Bruker Optics). A SHIMADZU UV-1800 spectrophotometer was used for UV-Vis measurements. MALDI-TOF-MS analyses were carried out using a 4800 MALDI TOF/TOF analyzer (AB SCIEX) equipped with a pulsed Nd:YAG laser at an excitation wavelength of 355 nm. For each MS spectrum, 1250 laser shots were fired (50 sub-spectra, 25 shots per sub-spectrum). The mass spectra analyzed using Data Explorer 4.9 software (AB SCIEX). GlycoWorkbench software was employed for MS data interpretation.

Results and Discussion

Characterization of Matrix Materials and Reproducibility of Acquired Signals

The optical and structural properties of CNPs and GNs were investigated by TEM, UV-Vis, and Raman spectroscopy analyses. TEM images of CNPs and GNs are shown in Figs. S1a and S1b, respectively. The TEM images display that the CNPs are monodisperse with average diameters of 50.7 ± 0.02 nm, whereas GNs possess a transparent sheet structure with an average thickness of 2.3 ± 0.07 nm and an average lateral size of 706.1 ± 0.03 nm. The UV-Vis absorption spectra (Fig. S1c) of CNPs and GNs indicated that both CNPs and GNs have a broad absorption peak from 250 to 375 nm (MALDI laser radiation at 355 nm, falls within this range), which corresponds to a π–π^* transition of aromatic sp^2 domains [20]. As can be observed, CNPs have a higher molar absorptivity over the UV-Vis region. Raman spectra of CNPs (Fig. S1d) and GNs (Fig. S1e) show a G-band at 1590 cm^{-1}, which is related to in-plane vibration of sp^2 carbons [35]. The results verified the π-conjugation structures of CNPs and GNs, which facilitate the absorption and transfer of laser energy.

In general, heterogeneous crystallization of matrix materials results in poor shot-to-shot reproducibility, and the signal to noise ratio of a MALDI mass spectrum is highly dependent on the spot that is irradiated by the laser. As can be seen in Figure 1a, DHB tends to form large needle-shaped crystals near the rim of the target plate, when using the dried-drop method at atmospheric pressure. Although crystallization was improved under the vacuum by minimizing the evaporation-driven flux [36, 37], still some small crystals formed near the rim (Figure 1b). In contrast, when CNPs were utilized as a matrix (Figure 1c) or co-matrix (Figure 1d), more homogeneous layers were formed. Comparable results were observed when GNs were used as a matrix (Figure 1e) or co-matrix (Figure 1f); however, due to the greater dispersibility of CNPs

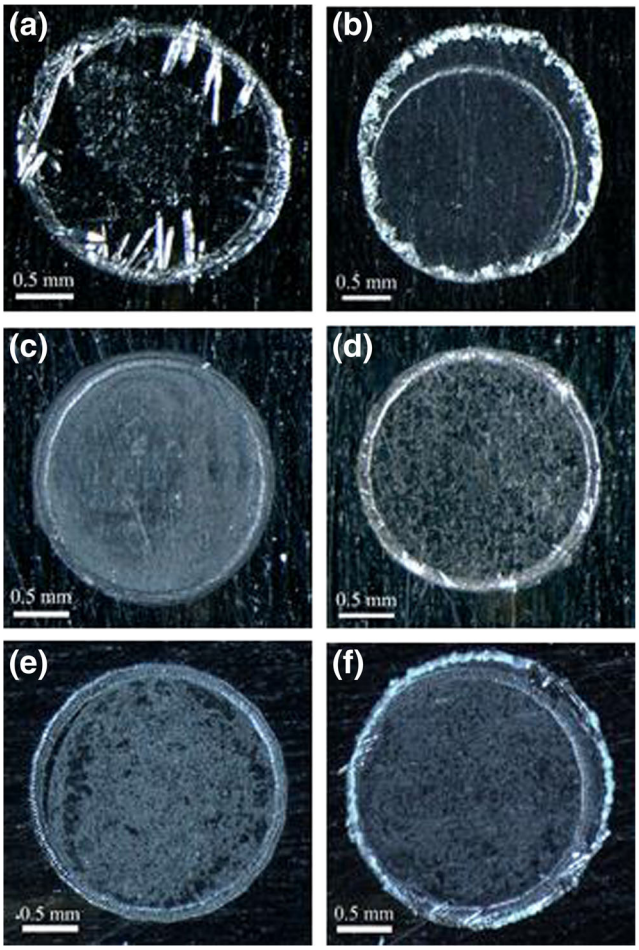

Figure 1. The optical images of the spots (**a**) DHB dried at atmospheric pressure, (**b**) DHB dried under vacuum, (**c**) CNPs dried at atmospheric pressure, (**d**) DHB + CNPs, dried at atmospheric pressure, (**e**) GNs dried at atmospheric pressure, (**f**) DHB + GNs, dried at atmospheric pressure

and their narrow particle size, matrix materials crystalized in a more homogenous fashion. To illustrate the poor reproducibility of DHB, N-glycans derived from RNase B (a model glycoprotein containing five high mannose structures) were investigated. The relative standard deviations (RSD) of the normalized peak heights for the five major glycoforms of RNase B were 22.9, 16.3, 10.3, 18.7, and 15.5, acquired five times by automatic measurements on a single spot. On the contrary, the RSD results for RNase B glycans using CNPs as co-matrix were 6.7, 4.6, 2.8, 5.2, and 4.1, which confirmed enhancement of shot-to-shot reproducibility.

Performance of Matrices for Glycan Profiling

In the interest of evaluating the performance of GNs and CNPs as MALDI matrices, N-glycans derived from 100 ng of RNase B were first chosen as a representative sample. Similar to the DHB, CNPs and GNs demonstrate interference-free backgrounds in the mass range that most glycans are found within, *m/z* 700–5000 (Fig. S2). Figure 2 depicts the obtained MS profiles with all corresponding glycan structures represented

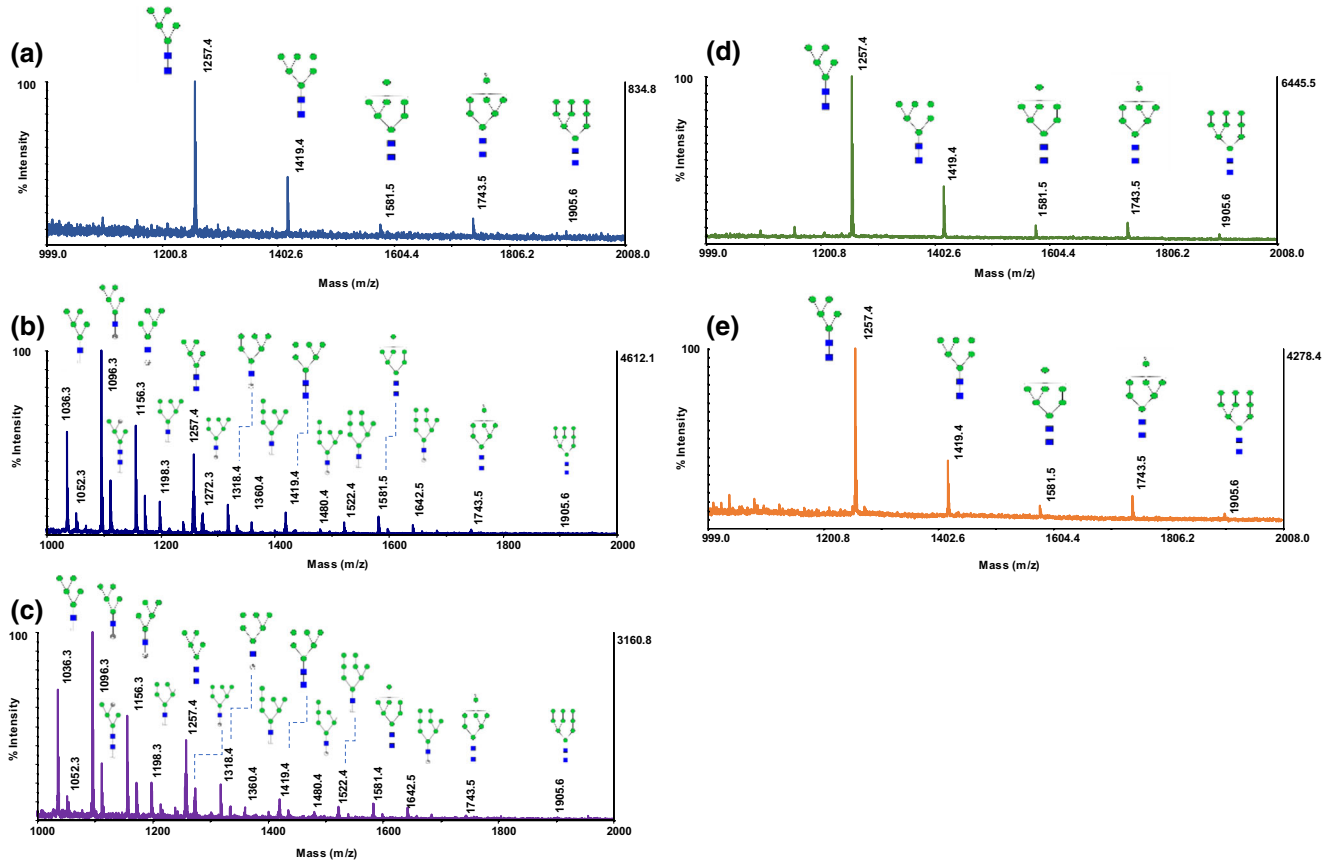

Figure 2. MALDI-TOF-MS profiles of N-glycans derived from 100 ng of RNase B using (**a**) 10 μg DHB, (**b**) 1 μg CNPs, (**c**) 1 μg GNs, (**d**) 10 μg DHB + 0.025 μg CNPs, (**e**) 10 μg DHB + 0.05 μg GNs. Symbols: ■, N-acetylglucosamine; ○, galactose; ▼, fucose; ●, mannose; ◆, N-acetylneuraminic acid

as cartoons. As can be seen in Figure 2a, the use of DHB, which is commonly used for MALDI analysis of glycans, resulted in the five high mannose glycans of RNase B being detected as $[M + Na]^+$ adducts at relatively low intensity. However, when CNPs (Figure 2b) and GNs (Figure 2c) were utilized as MALDI matrices improved, signal intensities were observed as well as ISD fragmentations that produced glycosidic and cross-ring cleavages. These observations are indicative of highly efficient energy absorption and transfer by the matrix materials. To investigate the possibility of controlling the degree of ISD during measurements, to obtain easily interpreted spectra, a lower concentration of matrix materials (Fig. S3a) and laser intensities (Fig. S3b) were used. As it is shown, the intensities and the number of detected peaks decreased with concentration and laser intensity, although the fragment ions are prominent in the spectra.

Further, to test the performance of GNs and CNPs as co-matrices, DHB was mixed with these carbon nanomaterials prior to MALDI analyses. The signal intensities were increased by several orders of magnitude, with almost no noticeable ISD fragmentation using either CNPs-DHB (Figure 2d) or GNs-DHB (Figure 2e) matrices. By comparison of the obtained results, CNPs-DHB demonstrated the best analytical performance with the highest signal-to-noise ratios. As it was discussed above, in comparison with GNs, CNPs have a higher laser adsorption efficiency and smaller particle size, which improves energy absorption and transfer. Moreover, the higher dispersibility of CNPs enhances MS sensitivity, through the formation of more homogeneous layers of analytes on the MALDI plate (Figure 1d) [20].

The correlations between the glycan concentrations and signal intensities are shown in Fig. S4a. The intensities related to Man5 structure were selected to depict the correlations. As can be seen, the signal intensity increases as the amount of spotted glycan sample increases. The data fit polynomial curves for N-glycans derived from 5 to 1 μg of RNase B with correlation coefficients (R^2) better than 0.99.

The effect of CNP and GN concentrations on glycan profiling, when used as co-matrices, were also investigated. Interestingly, by increasing the amount of CNPs (Figure 3a) and GNs (Figure 3b), signal intensities were improved with a simultaneous increase in the degree of ISD fragmentation. Extensive glycosidic and cross-ring cleavages were observed at higher concentrations of CNPs and GNs, whereas peaks indicative of five intact glycans dominated the spectra at lower concentrations. The relative abundances of RNase B glycans acquired using these matrices, at different concentrations, were compared with previously reported NMR data [38]. The data are shown in Figures 3c, d, for DBH-CNPs and DHB-GNs matrices, respectively. Although there are differences between the

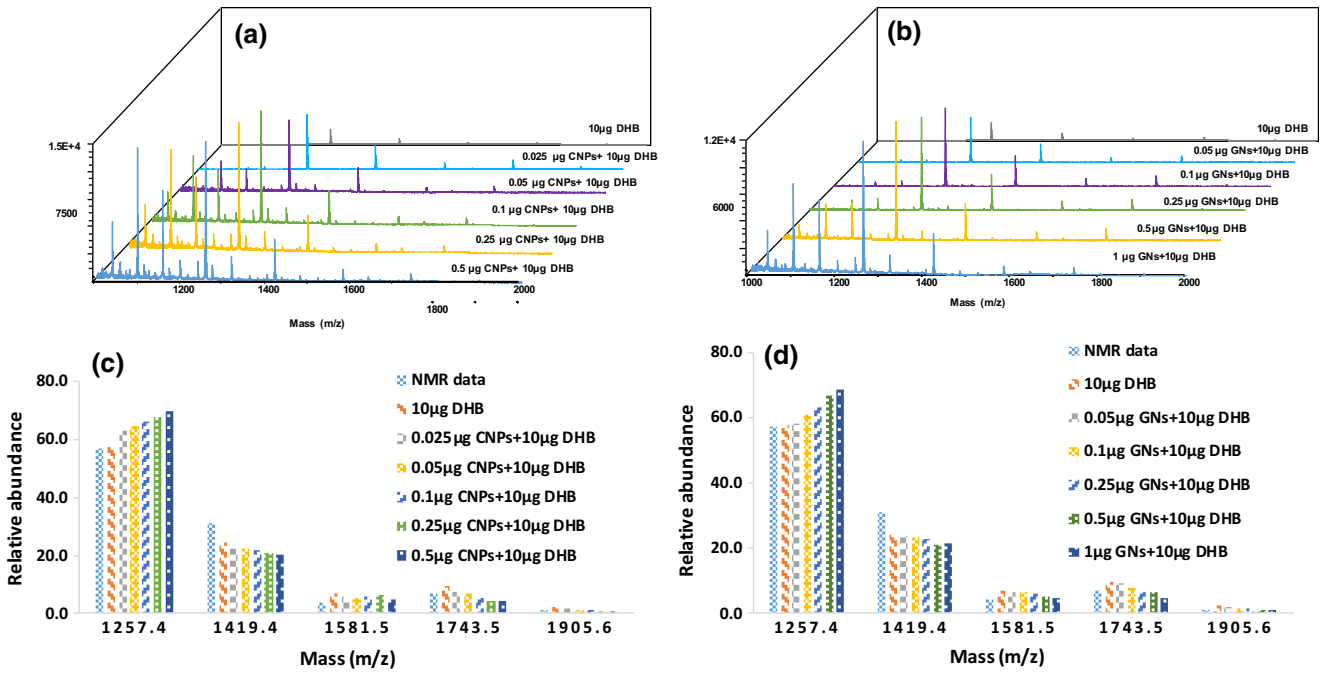

Figure 3. MALDI-TOF-MS profiles of RNase B glycans using DHB mixed with different amounts of (**a**) CNPs, (**b**) GNs. Relative abundance of RNase B glycans recorded using DHB mixed with different amounts of (**c**) CNPs and (**d**) GNs

results, such differences may be attributed to the source of RNase B samples and the measurement uncertainties inherent to the methods utilized. Moreover, the extensive fragmentation observed at higher concentrations of CNPs and GNs increased the abundance of HexNAc2Hex5 relative to other structures. The CNPs and GNs data are comparable to the NMR data, suggesting the applicability of the proposed matrices.

The results indicated that the degree of ISD fragmentation could be modulated by adjusting the concentration of CNPs or GNs added to the matrix. Figure 4a shows the obtained MS profile of N-glycans derived from 1 μg of RNase B, using 0.5 μg of CNPs as a co-matrix with DHB, which is sufficiently efficient to cause abundant cross-ring and glycosidic bond fragmentations with substantial intensities. The commonly observed Y-, B-ion series was present in addition to an A- and X-ion series, as well as some C-ions, for each of the five high mannose structures in the spectrum. Overall, the ions resulting from cross-ring fragmentation were more intense compared to those resulting from the cleavage of glycosidic bonds. The fragmented $^{0,2}A_5$ ions corresponding to the five high mannose structures are indicated in Figure 4a, as an example. The abundant A- and X-type ions are very informative for the study of linkages, for instance, A-type ions allow the distinction between α(1–4)- and α(1–6)-linked isobaric structures [39].

The ability to control ISD fragmentation allows the acquisition of pseudo-MS^3 experiments on instruments that do not have MS^n capabilities. Pseudo-MS^3 analysis is shown for *m/z*: 1096.3 (Figure 4b), 1318.4 (Figure 4c), 1156.3 (Fig. S5a), and 1036.3 (Fig. S5b), as representative ISD fragmented ions. Several ions corresponding to the fragmentation of the ions of interest were observed, with a relatively high signal to noise ratios, an aspect beneficial for structural analysis. Furthermore, it has previously been reported that ISD produces some low-intensity fragment ions when DHB is used as a MALDI matrix [31]. However, our results indicated that no peaks were observed in the pseudo-MS^3 profiles when the experiments were repeated using DHB. This further supports the hypothesis that CNPs and GNs may prove useful for pseudo-MS^3 structural characterization experiments.

Utility of the Binary Matrices for Various Types of Glycan Compounds

The applicability of the CNPs and GNs as MALDI matrices was further studied by investigating their efficiencies for the analysis of fetuin native glycans (a model glycoprotein containing sialylated glycans) and permethylated glycans derived from RNase B and fetuin. According to previous studies, direct analysis of native sialylated glycans is difficult, as the negative charge of sialic acid reduces the ionization efficiency in positive-ion mode and the non-derivatized sialic acid residues are often lost due to in- and post-source decay [19, 40]. Although negative-ion mode MS is proposed as an alternative option for MALDI analysis of native acidic glycans, it has been demonstrated that the sensitivity of sialylated glycans is at least 10 times less than neutral glycans when using DHB as a matrix [41]. The negative-ion mode MALDI-MS analysis results of N-glycans derived from 500 ng of fetuin using DHB as a matrix, exhibited weak signals with half of the glycan structures missing (Figure 5a), confirmed low ionization efficiency of the matrix. In contrast, MALDI-TOF mass spectra obtained in negative-ion mode under similar experimental conditions using CNPs and GNs as co-matrices are shown in Figure 5b and Fig. S4a. As can be seen, six glycan peaks originating from fully

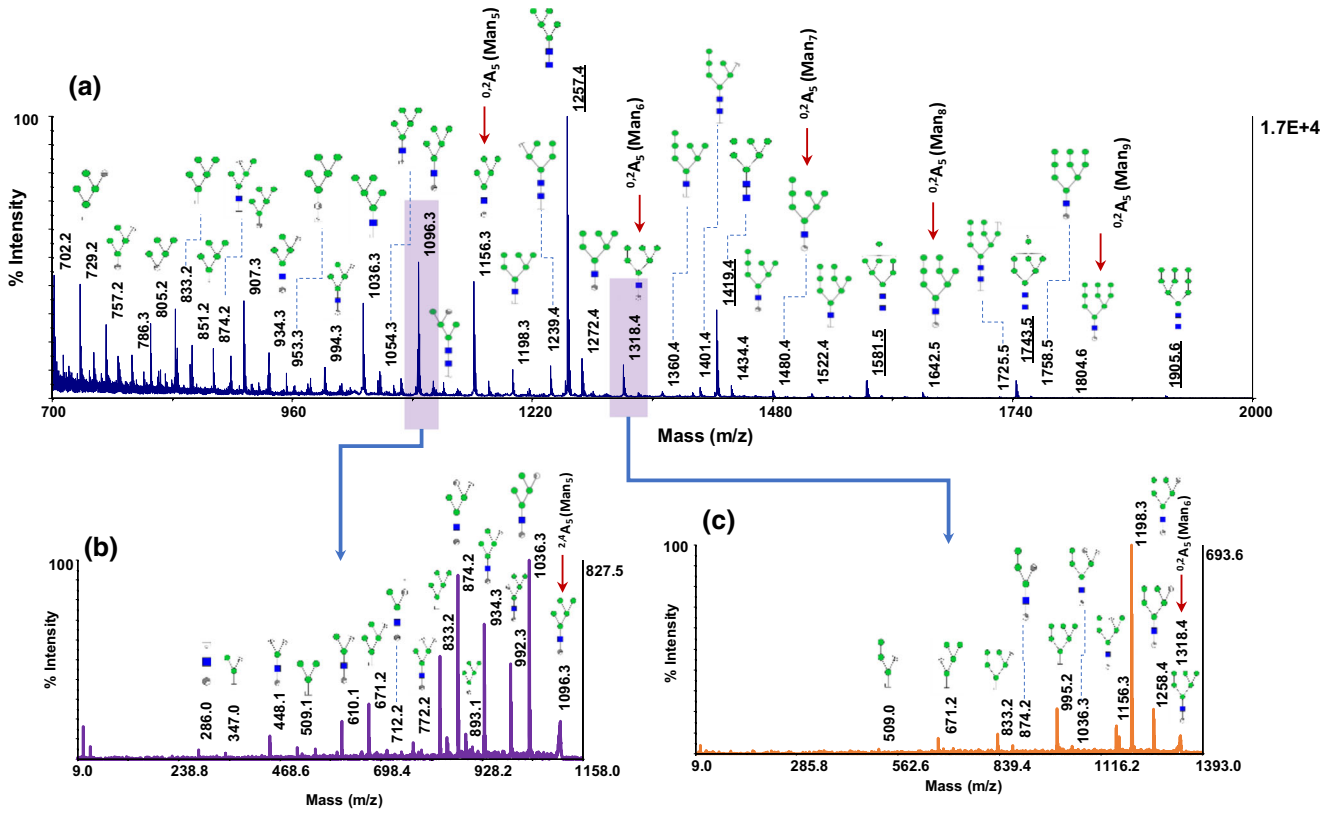

Figure 4. (**a**) MALDI-TOF-MS profile of N-glycans derived from 1 μg of RNase B using 10 μg DHB+ 0.5 μg CNPs. Underlines indicate the five intact high mannose structures and the arrows designate the fragmented $^{0,2}A_5$ ions corresponding to the five high mannose structures. (**b**) MS/MS spectrum of the ISD fragmented ion at *m/z* = 1096.3 and (**c**) MS/MS spectrum of the ISD fragmented ion at *m/z* = 1318.4. Symbols as in Fig. 2

and partially sialylated glycans were clearly detected as $[M\text{-}H]^{-1}$, $[M + Na\text{-}2H]^{-1}$, $[M\text{-}H]^{-1}$, $[M + Na\text{-}2H]^{-1}$, $[M + 2Na\text{-}3H]^{-1}$, and $[M + 3Na\text{-}4H]^{-1}$, respectively. These are the N-glycan structures known to exist in fetuin, and the intensities of their respective signals reflect the relative abundances in which they are commonly encountered [33, 42]. These results demonstrate that the proposed matrices are beneficial to the laser desorption/ionization process, which enhances measurement sensitivity in both positive- and negative-ion modes.

To date, permethylation is considered one of the most common derivatization methods in MS-based glycomic analyses [16, 33, 34, 43]. The procedure improves sensitivity in positive-ion mode by enhancing ionization efficiency and also substantially increase the stability of sialylated glycans. MS profiles of permethylated glycans derived from 100 ng of fetuin and RNase B were investigated to examine the performance of CNPs and GNs for the analysis of permethylated glycans (Figures 5 and S6). Although the signal intensities and the number of detected glycans were improved for permethylated glycans using DHB (Figures 5c, e), the signal intensities further increased by several orders of magnitude for both high mannose (Figures 5d and S4b) and sialylated glycans (Figures 5f and **S6c**) using CNPs or GNs as co-matrices.

The effect of CNP and GN concentrations was also investigated for permethylated glycans derived from RNase B as a model (Fig. S7). Similar to the native glycans, the signal intensities improved by increasing the amount of CNPs and GNs; however, no obvious fragmentations were detected at higher amounts of CNPs or GNs. According to the Asakawa et al. [44], the ISD fragments produced by hydrogen abstraction from the hydroxyl group of native glycans, create hydrogen-deficient glycan [M–H]·, prompting subsequent radical induced cleavage. The signal intensities were increased sharply up to the using 0.1 μg of CNPs or 0.25 μg GNs as co-matrix and reach almost plateau at higher concentrations of nanomaterials. Moreover, the relation between the concentration of permethylated glycan and signal intensity was tested using RNase B (Fig. S4b). The data fitted to the polynomial curves for premethylated glycans derived from 1 ng to 1 μg of RNase B.

Salt Tolerance of CNPs and GNs

Most biological samples contain a high concentration of salts which may affect ionization efficiency and suppress signal intensity in MALDI-TOF-MS analysis. Therefore, to enhance sensitivity in glycan profiling, purification and desalting of biological glycan samples are necessary prior MALDI analyses. Due to the unique interaction of carbon materials with both native and permethylated glycans, including hydrophobic, polar, and ionic interactions, they have been demonstrated to be an excellent class of sorbent

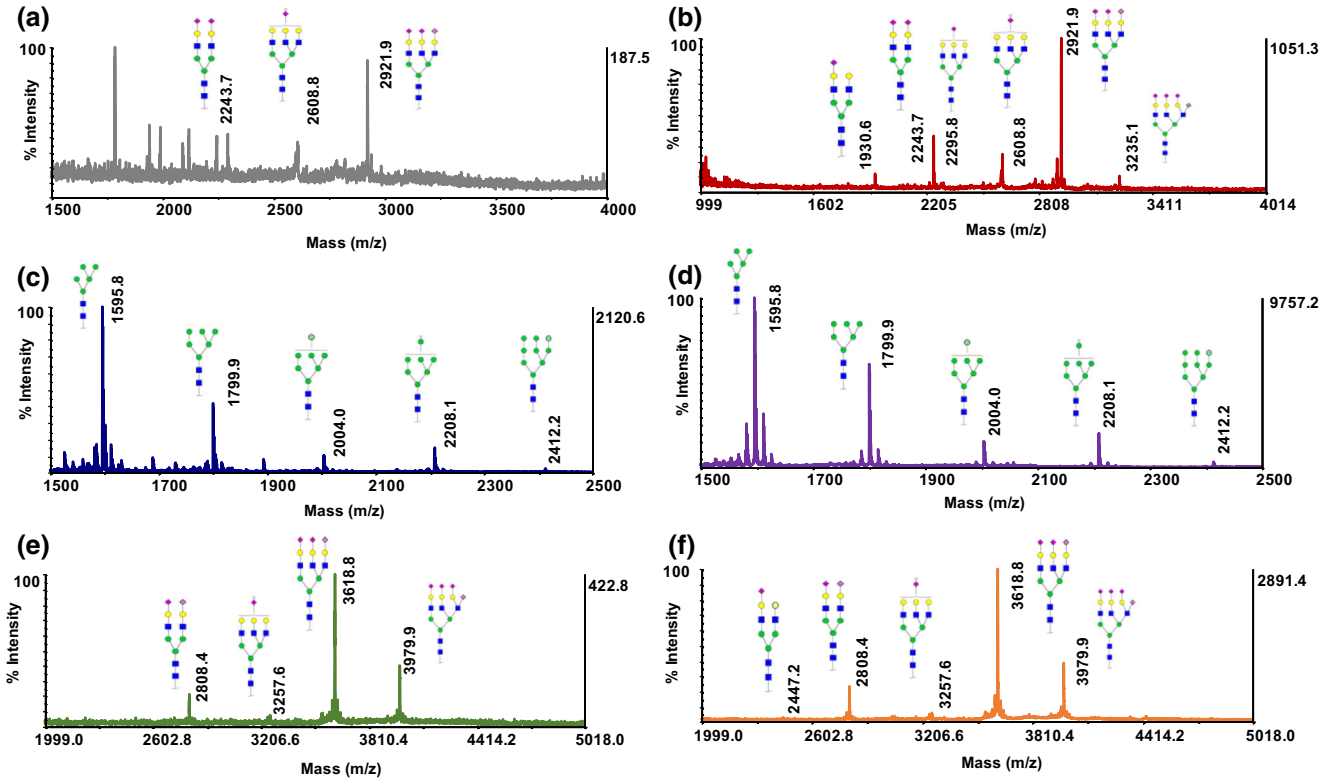

Figure 5. MALDI-TOF-MS profiles of (**a**) N-glycans derived from 500 ng of fetuin using 10 µg DHB, (**b**) N-glycans derived from 500 ng of fetuin using 10 µg DHB+ 0.025 CNPs, (**c**) permethylated N-glycans derived from 100 ng of RNase B, using 10 µg DHB, (**d**) permethylated N-glycans derived from 100 ng of RNase B, using 10 µg DHB+ 0.025 CNPs, (**e**) permethylated N-glycans derived from 100 ng of fetuin using 10 µg DHB, (**f**) permethylated N-glycans derived from 100 ng of fetuin, using 10 µg DHB+ 0.025 CNPs. Symbols as in Fig. 2

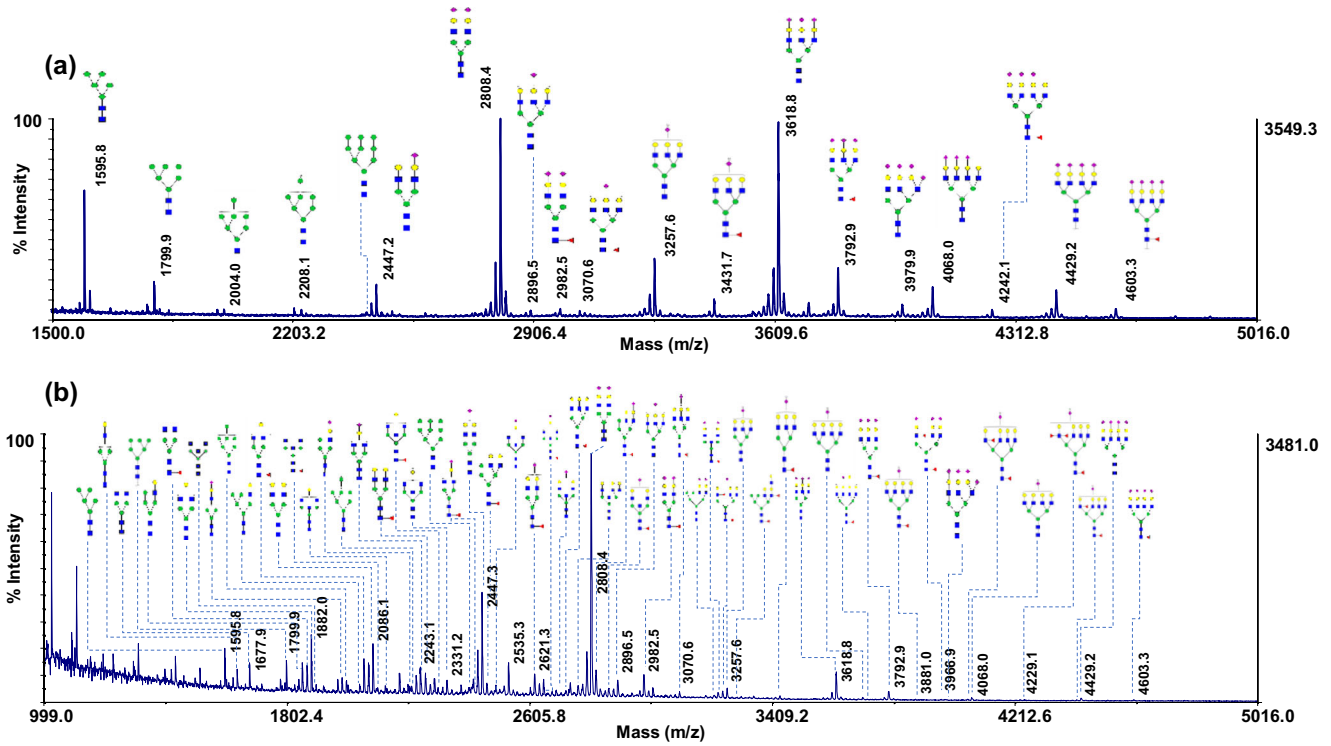

Figure 6. MALDI-TOF-MS profiles of purified and extracted permethylated glycans using CNPs, derived from (**a**) 0.8 µg mixture of RNase B, fetuin, and AGP with a 1:2:5 weigh ratio, respectively, (**b**) 10 µl of human blood serum. Symbols as in Fig. 2

materials for glycomic studies [45, 46]. The performance of CNPs and GNs was investigated for the profiling of glycan samples with high salt concentrations. For this purpose, both the native and permethylated glycan solutions were desalted via drop dialysis and liquid-liquid extraction, respectively, to remove salts that may have originated from buffers and/or derivatization reagents. NaCl was then added to the glycan samples, at predetermined concentrations, prior to the CNP and GN extraction process. Figure S8 depicts the MS profiles of native and permethylated glycans derived from RNase B, containing 500 mM NaCl, purified and extracted using CNPs (Figs. S8a and S8b) and GNs (Figs. S8c and S8d). All five of the RNase B glycan peaks were identified, confirming the high salt-tolerance capacity of CNPs and GNS as well as their enrichment and ionization ability. Moreover, as was shown in Fig. S8e, when DHB was used as a matrix, in the presence of 500 mM NaCl, signal intensity sharply decreased with three of the RNase B glycan structures undetected, demonstrating the weak salt tolerance of the matrix.

Due to the use of NaOH during the permethylation process, salts are always introduced into permethylated glycan samples, which results in poor MALDI ionization efficiency. Our data also confirmed the utility of CNPs and GNs for the direct analysis of permethylated glycans without the need for salt removal via liquid-liquid extraction. The results are shown in Figs. 6a and S9a for CNPs and GNs, respectively. As can be seen, all of the high mannose, sialylated, and fucosylated glycans were detected with an acceptable signal to noise ratios in the solution containing unpurified permethylated glycans derived from RNase B, Fetuin, and AGP. Again, confirming the dual capability of CNPs and GNs as enrichment adsorbents and MALDI matrices that offer an effective and fast technique for the detection of glycan molecules, while simplifying the process of sample pretreatment and isolation.

The performance of the CNPs and GNs was further investigated using human blood serum, as a complex biological sample. Human blood serum contains proteins with sophisticated glycosylation and its profiling plays an essential role in biomarker discovery and disease diagnosis and prognosis. MALDI-MS profiles of permethylated glycans derived from human blood serum samples, using CNPs and GNs for extraction and purification as well as co-matrices, are illustrated in Figures 6b and S9b. Similar patterns were observed, with 57 glycan structures confidently detected. In comparison with previously reported results for glycan profiling by MALDI analysis [47], the number of detected glycans substantially increased, mainly due to the high purification and ionization efficiencies of carbon nanomaterials.

Conclusion

In summary, CNPs and GNs were successfully used as MALDI matrices or co-matrices for glycan profiling of three diverse glycoproteins and human blood serum. Several advantages were observed that demonstrated their great potential to absorb glycans for purification and to act as an excellent medium for the transfer of laser energy to glycan analytes for MALDI-MS analyses. The aforementioned advantages include low background interference, improved signal intensities, high salt tolerance capacity, and enhancement of shot-to-shot reproducibility. CNP and GN concentrations can be adjusted to easily control the degree of glycosidic and cross-ring fragmentation. This level of control allows for comprehensive structural analysis through the simultaneous study of intact and fragmented glycans, as well as pseudo-MS^3 analyses.

Acknowledgments

This work was supported by an NIH grant (1R01GM112490-04).

References

1. Abou-Abbass, H., Abou-El-Hassan, H., Bahmad, H., Zibara, K., Zebian, A., Youssef, R., Ismail, J., Zhu, R., Zhou, S., Dong, X., Nasser, M., Bahmad, M., Darwish, H., Mechref, Y., Kobeissy, F.: Glycosylation and other PTMs alterations in neurodegenerative diseases: current status and future role in neurotrauma. Electrophoresis. **37**, 1549–1561 (2016)
2. Banazadeh, A., Veillon, L., Wooding, K.M., Zabet-Moghaddam, M., Mechref, Y.: Recent advances in mass spectrometric analysis of glycoproteins. Electrophoresis. **38**, 162–189 (2017)
3. Mechref, Y., Hu, Y., Desantos-Garcia, J.L., Hussein, A., Tang, H.: Quantitative glycomics strategies. Mol. Cell. Proteomics. **12**, 874–884 (2013)
4. Mechref, Y., Hu, Y., Garcia, A., Hussein, A.: Identifying cancer biomarkers by mass spectrometry-based glycomics. Electrophoresis. **33**, 1755–1767 (2012)
5. Mechref, Y., Hu, Y., Garcia, A., Zhou, S., Desantos-Garcia, J.L., Hussein, A.: Defining putative glycan cancer biomarkers by MS. Bioanalysis. **4**, 2457–2469 (2012)
6. Song, E., Mechref, Y.: Defining glycoprotein cancer biomarkers by MS in conjunction with glycoprotein enrichment. Biomark. Med. **9**, 835–844 (2015)
7. Albrecht, S., Mittermayr, S., Smith, J., Martin, S.M., Doherty, M., Bones, J.: Twoplex 12/13 C6 aniline stable isotope and linkage-specific sialic acid labeling 2D-LC-MS workflow for quantitative N-glycomics. Proteomics. **17**, (2017). https://doi.org/10.1002/pmic.201600304
8. Cheng, C.W., Chou, C.C., Hsieh, H.W., Tu, Z., Lin, C.H., Nycholat, C., Fukuda, M., Khoo, K.H.: Efficient mapping of sulfated Glycotopes by negative ion mode nanoLC-MS/MS-based Sulfoglycomic analysis of Permethylated Glycans. Anal. Chem. **87**, 6380–6388 (2015)
9. Lauber, M.A., Yu, Y.Q., Brousmiche, D.W., Hua, Z., Koza, S.M., Magnelli, P., Guthrie, E., Taron, C.H., Fountain, K.J.: Rapid preparation of released N-Glycans for HILIC analysis using a labeling reagent that facilitates sensitive fluorescence and ESI-MS detection. Anal. Chem. **87**, 5401–5409 (2015)
10. Liu, S., Gao, W., Wang, Y., He, Z., Feng, X., Liu, B.F., Liu, X.: Comprehensive N-glycan profiling of Cetuximab biosimilar candidate by NP-HPLC and MALDI-MS. PLoS One. **12**, e0170013 (2017)
11. Snyder, C.M., Alley Jr., W.R., Campos, M.I., Svoboda, M., Goetz, J.A., Vasseur, J.A., Jacobson, S.C., Novotny, M.V.: Complementary Glycomic analyses of sera derived from colorectal Cancer patients by MALDI-TOF-MS and microchip electrophoresis. Anal. Chem. **88**, 9597–9605 (2016)
12. Song, X., Ju, H., Lasanajak, Y., Kudelka, M.R., Smith, D.F., Cummings, R.D.: Oxidative release of natural glycans for functional glycomics. Nat. Methods. **13**, 528–534 (2016)
13. Veillon, L., Huang, Y., Peng, W., Dong, X., Cho, B.G., Mechref, Y.: Characterization of isomeric glycan structures by LC-MS/MS. Electrophoresis. **38**, 2100–2114 (2017)

14. Wooding, K.M., Peng, W., Mechref, Y.: Characterization of pharmaceutical IgG and Biosimilars using miniaturized platforms and LC-MS/MS. Curr. Pharm. Biotechnol. **17**, 788–801 (2016)
15. Zhao, J., Li, S., Li, C., Wu, S.L., Xu, W., Chen, Y., Shameem, M., Richardson, D., Li, H.: Identification of low abundant isomeric N-glycan structures in biological therapeutics by LC/MS. Anal. Chem. **88**, 7049–7059 (2016)
16. Zhou, S., Hu, Y., Veillon, L., Snovida, S.I., Rogers, J.C., Saba, J., Mechref, Y.: Quantitative LC-MS/MS Glycomic analysis of biological samples using AminoxyTMT. Anal. Chem. **88**, 7515–7522 (2016)
17. Zhou, S., Huang, Y., Dong, X., Peng, W., Veillon, L., Kitagawa, D.A.S., Aquino, A.J.A., Mechref, Y.: Isomeric separation of Permethylated Glycans by porous graphitic carbon (PGC)-LC-MS/MS at high temperatures. Anal. Chem. **89**, 6590–6597 (2017)
18. Qin, H., Zhao, L., Li, R., Wu, R., Zou, H.: Size-selective enrichment of N-linked glycans using highly ordered mesoporous carbon material and detection by MALDI-TOF MS. Anal. Chem. **83**, 7721–7728 (2011)
19. Zhou, H., Warren, P.G., Froehlich, J.W., Lee, R.S.: Dual modifications strategy to quantify neutral and sialylated N-glycans simultaneously by MALDI-MS. Anal. Chem. **86**, 6277–6284 (2014)
20. Chen, S., Zheng, H., Wang, J., Hou, J., He, Q., Liu, H., Xiong, C., Kong, X., Nie, Z.: Carbon nanodots as a matrix for the analysis of low-molecular-weight molecules in both positive- and negative-ion matrix-assisted laser desorption/ionization time-of-flight mass spectrometry and quantification of glucose and uric acid in real samples. Anal. Chem. **85**, 6646–6652 (2013)
21. Chen, Y., Gao, D., Bai, H., Liu, H., Lin, S., Jiang, Y.: Carbon dots and 9AA as a binary matrix for the detection of small molecules by matrix-assisted laser desorption/ionization mass spectrometry. J. Am. Soc. Mass Spectrom. **27**, 1227–1235 (2016)
22. Gulbakan, B., Yasun, E., Shukoor, M.I., Zhu, Z., You, M., Tan, X., Sanchez, H., Powell, D.H., Dai, H., Tan, W.: A dual platform for selective analyte enrichment and ionization in mass spectrometry using aptamer-conjugated graphene oxide. J. Am. Chem. Soc. **132**, 17408–17410 (2010)
23. Liu, Q., Cheng, M., Wang, J., Jiang, G.: Graphene oxide nanoribbons: improved synthesis and application in MALDI mass spectrometry. Chemistry. **21**, 5594–5599 (2015)
24. Liu, Y., Liu, J., Deng, C., Zhang, X.: Graphene and graphene oxide: two ideal choices for the enrichment and ionization of long-chain fatty acids free from matrix-assisted laser desorption/ionization matrix interference. Rapid Commun. Mass Spectrom. **25**, 3223–3234 (2011)
25. Lu, M., Lai, Y., Chen, G., Cai, Z.: Matrix interference-free method for the analysis of small molecules by using negative ion laser desorption/ionization on graphene flakes. Anal. Chem. **83**, 3161–3169 (2011)
26. Lu, W., Li, Y., Li, R., Shuang, S., Dong, C., Cai, Z.: Facile synthesis of N-doped carbon dots as a new matrix for detection of Hydroxy-polycyclic aromatic hydrocarbons by negative-ion matrix-assisted laser desorption/ionization time-of-flight mass spectrometry. ACS Appl. Mater. Interfaces. **8**, 12976–12984 (2016)
27. Rodriguez, C.E., Palacios, J., Fajardo, I., Urdiales, J.L., Le Guevel, X., Lozano, J., Sanchez-Jimenez, F.: Conventional matrices loaded onto a graphene layer enhances MALDI-TOF/TOF signal: its application to improve detection of phosphorylated peptides. J. Am. Soc. Mass Spectrom. **27**, 366–369 (2016)
28. Tang, L.A., Wang, J., Loh, K.P.: Graphene-based SELDI probe with ultrahigh extraction and sensitivity for DNA oligomer. J. Am. Chem. Soc. **132**, 10976–10977 (2010)
29. Lee, J., Kim, Y.K., Min, D.H.: Laser desorption/ionization mass spectrometric assay for phospholipase activity based on graphene oxide/carbon nanotube double-layer films. J. Am. Chem. Soc. **132**, 14714–14717 (2010)
30. Wang, J., Liu, Q., Liang, Y., Jiang, G.: Recent progress in application of carbon nanomaterials in laser desorption/ionization mass spectrometry. Anal. Bioanal. Chem. **408**, 2861–2873 (2016)
31. Smargiasso, N., De Pauw, E.: Optimization of matrix conditions for the control of MALDI in-source decay of permethylated glycans. Anal. Chem. **82**, 9248–9253 (2010)
32. Liang, Q., Macher, T., Xu, Y., Bao, Y., Cassady, C.J.: MALDI MS in-source decay of glycans using a glutathione-capped iron oxide nanoparticle matrix. Anal. Chem. **86**, 8496–8503 (2014)
33. Zhou, S., Dong, X., Veillon, L., Huang, Y., Mechref, Y.: LC-MS/MS analysis of permethylated N-glycans facilitating isomeric characterization. Anal. Bioanal. Chem. **409**, 453–466 (2017)
34. Zhou, S., Wooding, K.M., Mechref, Y.: Analysis of Permethylated glycan by liquid chromatography (LC) and mass spectrometry (MS). Methods Mol. Biol. **1503**, 83–96 (2017)
35. Krishnamoorthy, K., Veerapandian, M., Yun, K., Kim, S.J.: The chemical and structural analysis of graphene oxide with different degrees of oxidation. Carbon. **53**, 38–49 (2013)
36. Cohen, S.L., Chait, B.T.: Influence of matrix solution conditions on the MALDI-MS analysis of peptides and proteins. Anal. Chem. **68**, 31–37 (1996)
37. Shin, D., Kim, I., Paek, J., Kim, J.: A novel "freeze vacuum drying" crystallization method toward quantitative MALDI-MS. Bull. Kor. Chem. Soc. **38**, 133–135 (2017)
38. Fu, D., Chen, L., O'Neill, R.A.: A detailed structural characterization of ribonuclease B oligosaccharides by 1H NMR spectroscopy and mass spectrometry. Carbohydr. Res. **261**, 173–186 (1994)
39. Mechref, Y., Novotny, M.V., Krishnan, C.: Structural characterization of oligosaccharides using MALDI-TOF/TOF tandem mass spectrometry. Anal. Chem. **75**, 4895–4903 (2003)
40. Harvey, D.J.: Analysis of carbohydrates and glycoconjugates by matrix-assisted laser desorption/ionization mass spectrometry: an update for 2011–2012. Mass Spectrom. Rev. **36**, 255–422 (2017)
41. Mechref, Y., Novotny, M.V.: Matrix-assisted laser desorption/ionization mass spectrometry of acidic glycoconjugates facilitated by the use of spermine as a co-matrix. J. Am. Soc. Mass Spectrom. **9**, 1293–1302 (1998)
42. Green, E.D., Adelt, G., Baenziger, J.U., Wilson, S., Van Halbeek, H.: The asparagine-linked oligosaccharides on bovine fetuin. Structural analysis of N-glycanase-released oligosaccharides by 500-megahertz 1H NMR spectroscopy. J. Biol. Chem. **263**, 18253–18268 (1988)
43. Hu, Y., Shihab, T., Zhou, S., Wooding, K., Mechref, Y.: LC-MS/MS of permethylated N-glycans derived from model and human blood serum glycoproteins. Electrophoresis. **37**, 1498–1505 (2016)
44. Asakawa, D., Smargiasso, N., De Pauw, E.: Identification and relative-quantification of glycans by matrix-assisted laser desorption/ionization in-source decay with hydrogen abstraction. Anal. Chem. **84**, 7463–7468 (2012)
45. Melmer, M., Stangler, T., Premstaller, A., Lindner, W.: Comparison of hydrophilic-interaction, reversed-phase and porous graphitic carbon chromatography for glycan analysis. J. Chromatogr. A. **1218**, 118–123 (2011)
46. Ruhaak, L.R., Deelder, A.M., Wuhrer, M.: Oligosaccharide analysis by graphitized carbon liquid chromatography-mass spectrometry. Anal. Bioanal. Chem. **394**, 163–174 (2009)
47. Hu, Y., Mechref, Y.: Comparing MALDI-MS, RP-LC-MALDI-MS and RP-LC-ESI-MS glycomic profiles of permethylated N-glycans derived from model glycoproteins and human blood serum. Electrophoresis. **33**, 1768–1777 (2012)